JOURNAL OF MATERIALS SCIENCE 26 (1991) 2900–2906

Laser irradiation studies of Te–Se–Br glasses

J. L. ADAM *, C. ORTIZ, J. R. SALEM
IBM Research Division, Almaden Research Center, 650 Harry Road, San Jose, CA 95120-6099, USA

X. H. ZHANG
Laboratoire de Chimie Minérale D, Unité Associée au C.N.R.S. No. 254, Université de Rennes I, Avenue du Général Leclerc, 35042 Rennes Cedex, France

We have studied the effect of laser irradiation on Te–Se–Br thin films. The major effect has been found to be dominated by changes in composition which include different morphologies. These changes are analysed by quantitative transmission electron microscopy (TEM) and scanning electron microscopy (SEM) as well as real time optical reflectivity. The measured losses of Br and Se are reasonable in view of the temperatures obtained from heat flow calculations for different laser pulse length and laser power conditions. When crystallization occurs, we have been able to establish that it starts with surface filamentary growth which exhibits fractal network formation. With higher laser energy, the filaments tend to coalesce to form metallic three dimensional crystals.

1. Introduction

First based on two elements, Te and Cl, chalco-halide glasses have been found to vitrify in a number of binary and ternary systems comprised of Te–Cl, Br or I–Se or S [1]. They belong to a totally new class of infrared-transmitting glasses and, because they transmit the 10.6 μm line of the CO_2 laser, can be drawn into fibres [2] and can be deposited as thin films [3], these materials are very promising candidates for infrared (IR) optical applications. The structure of these chalco-halide glasses is very likely derived from their crystalline counterparts such as Te_2Br and Te_3Cl_2 which exhibit infinite spiralling chains of tellurium and whose structure was determined by Kniep *et al.* [4]. Disorder can easily take place in these chains by rotation along the Te–Te bond [1]. The addition of a third element such as Se increases the disorder and stabilizes the glass phase. In the present study, we report, for the first time, the structural changes induced by laser irradiation in these materials, specifically in a Te–Se–Br thin film. Amorphous and crystalline phases are formed and their chemical composition is determined.

2. Experimental procedure

2.1. Target and thin film preparation

All targets were cast from material having a starting composition of $Te_{30}Se_{50}Br_{20}$. This material was prepared as described in detail elsewhere [1]. The targets were cast as 3–5 mm thick, 25 mm diameter discs and annealed slightly below the glass temperature (75 °C) to remove internal stress. Glass temperatures were measured by using a Dupont model 910 differential scanning calorimeter (DSC) with a 10 °C min^{-1} heating rate.

Because of the low glass temperature and very large thermal coefficient of expansion ($\simeq 5 \times 10^{-5}\ K^{-1}$), the targets were neither indium soldered nor epoxy bonded to the sputter cathode as is usual practice. They were, instead, secured by a stainless steel clamp ring. This ring was shielded from ion bombardment by a ground shield. The radio frequency (R.F.) diode sputtering system was evacuated to a pressure of less than 7×10^{-6} Pa prior to deposition. During deposition the argon pressure and R.F. power levels were 2Pa and 30 watts, respectively.

2.2. Thin film irradiation

The experimental set-up is illustrated in Fig. 1. The sample was mounted within a vacuum chamber capable of a base pressure of 5×10^{-5} Pa. The 514.5 nm sample irradiation pulses were produced as follows: Light from the argon ion laser (Coherent Radiation Innova 90) was chopped by an Isomet model 1211 acousto-optic modulator to produce discrete pulses of variable length. Beam position and focus (10 μm FWHM) was implemented with a three axis motorized stage (x,y axis: position, z axis: focus) driven by an Oriel Encoder-Mike controller model 18011. A general purpose interface bus enabled the laser power, pulse width, and beam position to be controlled by an IBM PS/2 computer.

* *Permanent address*: Laboratoire de Chimie Minérale D, Unité Associée au C.N.R.S. No. 254, Université de Rennes I, Avenue du Général Leclerc, 35042 Rennes Cedex, France.

0022–2461/91 $03.00 + .12

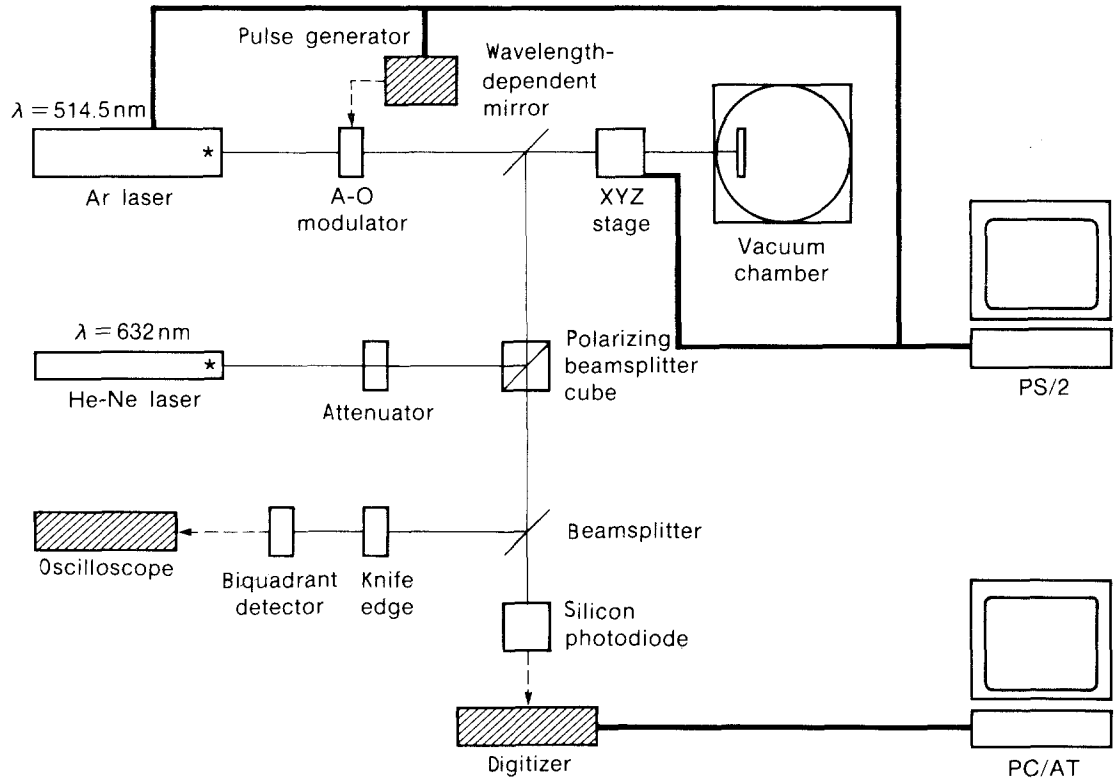

Figure 1 Experimental set-up for laser irradiation and reflectivity measurement of thin films.

2.3. Focus and reflectivity measurements

A dichroic mirror enabled a 632 nm beam from a 15 mW Melles Griot He–Ne laser to be combined colinear with the 514.5 nm irradiation pulse. The reflected light from the He–Ne was divided along two paths. Part of the light was sent to a Foulcault tester with a biquadrant photo-detector output. The optical path is such, that when the beam is focused at the sample, it is also focused at the knife edge and both sides of the detector are equally illuminated.

The second 632 nm beam was used for a real time reflectivity measurement. This light was collected on a fast PIN diode detector. The signal was amplified and fed to a Sequence model 3000 waveform digitizer. The digitizer was triggered by a Hewlett-Packard model 8112A pulse generator. This pulse generator also provided the pulse burst to drive the acousto-optic modulator mentioned earlier. The output of the digitizer was down loaded into an IBM PC/AT computer for data manipulation and hard copy production *via* a printer.

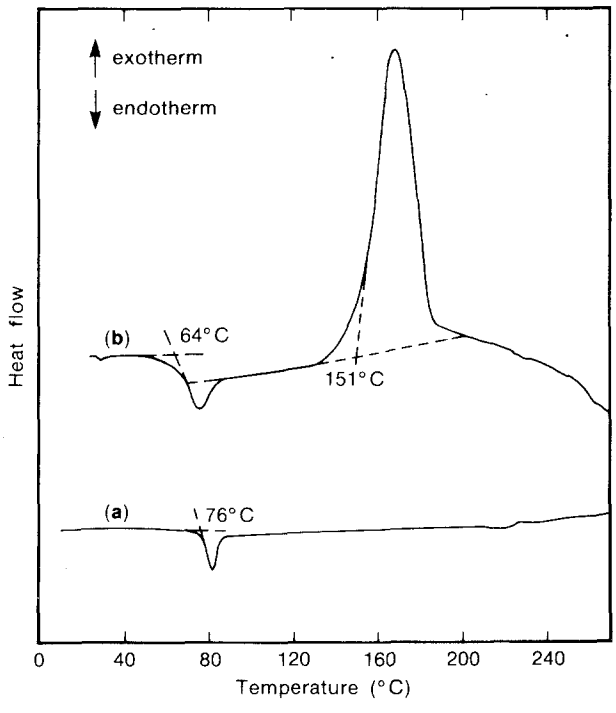

Figure 2 DSC curves for (a) $Te_{30}Se_{50}Br_{20}$ (target) and (b) $Te_{36}Se_{51}Br_{13}$ glasses.

2.4. Structure and composition analyses

After irradiation, the thin films have been analysed by TEM and energy dispersive spectroscopy (EDS). TEM observations have been carried out on a Philips model 301 electron microscope. EDS has been conducted at the National Center for Electron Microscopy (University of California, Berkeley) by means of a Jeol model JEM 200CX analytical electron microscope with a Kevex system 8000 attachment. The beam probe was 60 nm in diameter.

3. Results

The results of differential scanning calorimetry for the target ($Te_{30}Se_{50}Br_{20}$) are shown in Fig. 2a. The lack of crystallization peaks indicates that this composition is very stable in the glassy state, with little tendency to become an ordered material. As mentioned earlier [3], sputtering of this type of material induces a loss of halogen. The composition of the as-deposited film has

been analysed by electron microprobe and was found to be $Te_{36}Se_{51}Br_{13}$ indicating loss of both Se and Br. A DSC scan of a bulk sample with a similar composition (Fig. 2b) shows that, contrary to the target composition, the thin films can exhibit crystallization at 150 °C. Thus, structural phase transitions may be expected from this particular glassy alloy and hence our thin films.

We have performed laser irradiation of a 50 nm thick film whose initial composition is $Te_{36}Se_{51}Br_{13}$. By measuring the transmission spectrum and reflectivity of the various layers of our system (thin film/carbon/mica) we have estimated that the ratio of laser power absorbed by the film to incident power was approximately 35%. In the remainder of this paper, the power quoted is the laser power absorbed by the film. Our study covers absorbed laser powers ranging from 20 to 150 mW and laser pulse lengths from 700 ns to 1s. Depending on these two parameters, morphological changes may or may not occur in the thin film. Our observations are summarized in the irradiation diagram shown in Fig. 3, where one can distinguish four regions:

1. Region I, for which the total energy density absorbed during the pulse duration is too small to induce any morphology changes.

2. Region II, which can be identified as the short pulse–high power region. Pulses are from 700 ns to 100 μs long while absorbed power ranges from 150 to 12 mW. In this region, the amount of energy absorbed is large enough to modify the morphology of the film.

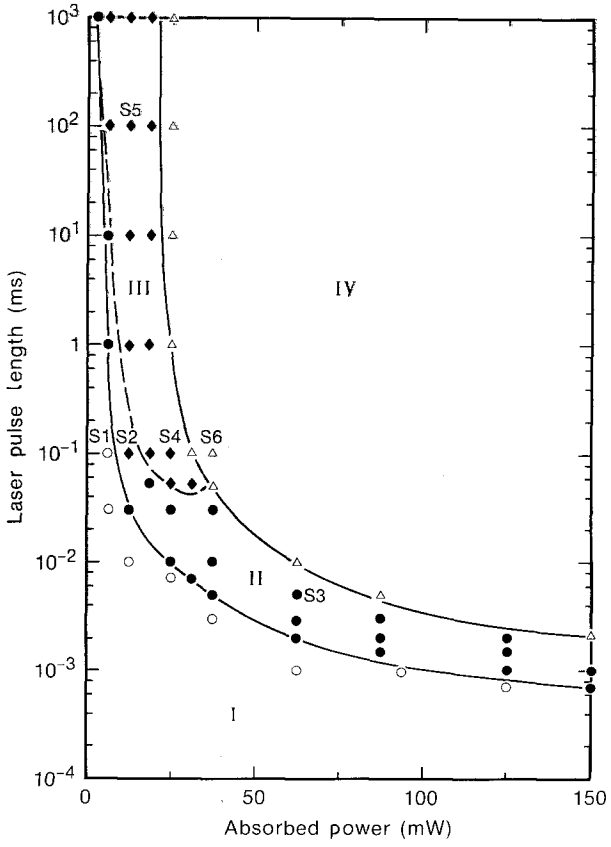

Figure 3 Morphology of a $Te_{36}Se_{51}Br_{13}$ thin film (50 nm) as a function of laser power and pulse length. (I, ○) no evolution, amorphous. (II, ●) morphology change, mostly amorphous with a few crystals. (III, ◆) crystalline. (IV, △) ablated.

However, most of the irradiated areas have been found to be still amorphous with a few superficial crystals. One can easily suggest that lattice ordering does not have time to occur and consequently no crystallization is observed.

3. Region III, identified as the long pulse–low power region. Pulse duration ranges from 50 μs to 1s and absorbed laser power from 31 to 6 mW. Here the amount of energy is high enough to induce visible morphology changes and in addition, crystal formation in large areas has time to take place.

4. Region IV, for which the total amount of energy absorbed during the pulse duration is so high that film ablation occurs.

Regions II and III contain the main important features of the laser irradiation. The experimental conditions referred to as S1 to S6 in Fig. 3 will be discussed in more detail later. We have repeated these investigations for a thicker film (300 nm). In that case the pulse power diagram is similar in shape to the one discussed above. The main difference is that, as expected, longer pulses are needed to achieve either crystallization or ablation.

Typical TEM pictures for irradiated spots S2 (12 mW, 100 μs), S3 (62 mW, 5 μs), S4 (25 mW, 100 μs) and S5 (12 mW, 100 ms) are shown in Fig. 4a–d, respectively. By use of selected area diffraction (SAD) we have determined that the irradiated areas in Fig. 4a and b were amorphous. However, by using microdiffraction some of the filamentary growth that are observed at the surface of the film in Fig. 4a are found to be monocrystalline. This is considered the first step of crystallization induced by laser irradiation in these materials. Fig. 4b is a more advanced step where filamentaries are absent from the centre of the spot. It is likely that because of the higher energy density absorbed, the filamentary structures have coalesced into the observed three dimensional metallic Se–Te particles. In the outer ring on the contrary, where the temperature is lower, dendritic growth is still observed. In Fig. 4c, the dark particles in the irradiated spot are found to be crystals while the lighter back ground is amorphous. The dark wavy edge of the spot is also crystalline. In Fig. 4d, the spot is crystalline except the bright area in the centre which is amorphous. The gradation of black and grays in the outermost crystalline area is not due to composition changes but to contrast induced by crystal orientation.

Using EDS, the chemical composition of the spots of Fig. 4b–d described above and of the as-deposited film have been determined and are shown in Table I. In some cases, impurities such as Fe and Si have been detected. Their concentration was in the 1 at % range. Since no relationship has been found between the presence of such impurities and the occurrence of crystallization, we have omitted these two elements in our analysis. When analysing the different crystalline regions, we can always index the structure as hexagonal. After irradiation the bromine content is very low. Since the chemical analysis by EDS shows different compositions and both Te and Se crystallize in the hexagonal system, we conclude that the crystals

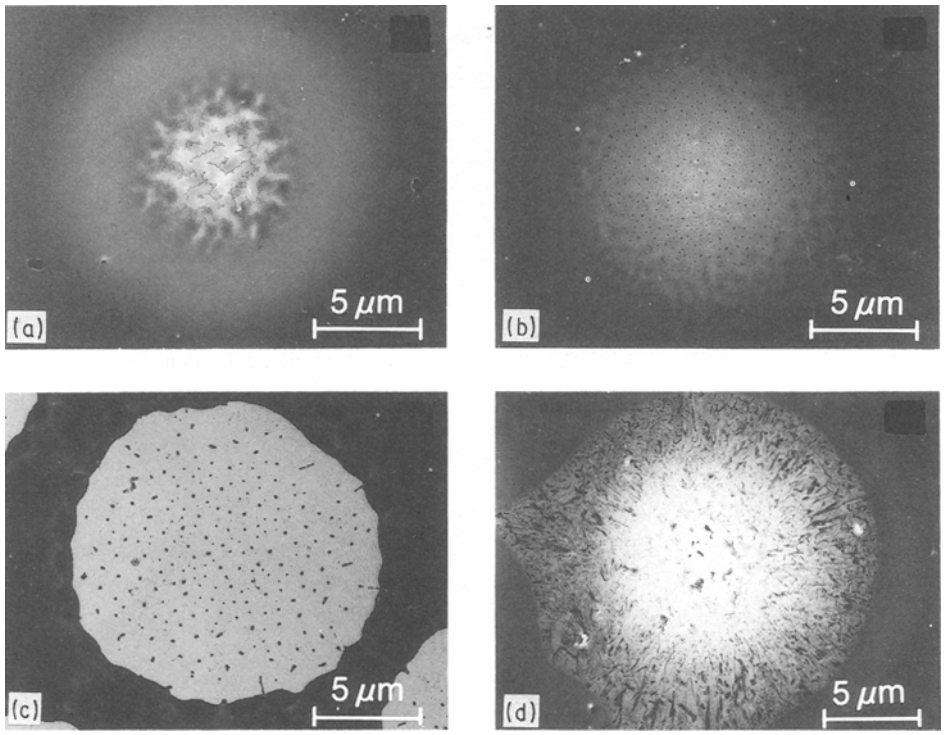

Figure 4 Irradiated thin film of initial composition $Te_{36}Se_{51}Br_{13}$; (a) S2 (12 mW, 100 μs), mainly amorphous. (b) S3 (62 mW, 5 μs), mainly amorphous. (c) S4 (25 mW, 100 μs), partly crystalline. (d) S5 (12 mW, 100 ms), crystalline. Laser beam diameter is 10 μm (FWHM).

TABLE I EDS analysis of irradiated $Te_{36}Se_{51}Br_{13}$ thin films

Sample	Morphology	Structure	Te (at %)	Se (at %)	Br (at %)
As-deposited		Amorphous	35.9	50.3	13.8
S3 (62 mW, 5 μs) Fig. 4b	Black particles in centre	Amorphous	70.1	29.2	0.7
	Bright background	Amorphous	[a]	[a]	[a]
	Dark areas in edge	Amorphous	57.7	42.3	0
S4 (25 mW, 100 μs) Fig. 4c	Black particles in centre	Crystalline	95.0	4.2	0.8
	Bright background	Amorphous	[a]	[a]	[a]
	Dark wavy edge	Crystalline	66.9	33.1	0
S5 (12 mW, 100 ms) Fig. 4d	Black particles in centre	Crystalline	92.9	7.1	0
	Bright areas in centre	Amorphous	[a]	[a]	[a]
	Outer ring	Crystalline	41.5	58.5	0

[a] All three elements are present. However the film is very thin in this region and consequently quantitative results are meaningless.

studied are formed by different solid solutions of Te and Se. In fact, in previous reports these elements have been found to be miscible in all proportions [5, 6].

From these results, one can conclude that the presence or absence of Br is not related to the amorphous or crystalline structure of the thin film. Also there is no obvious relation between the crystalline or amorphous character and the final Te/Se ratio.

Real time reflectivity measurements have been carried out for various irradiated spots in Region II and III of Fig. 3. A typical experimental curve is shown in Fig. 5 for a S3 (62 mW, 5 μs) laser pulse. A significant delay between time $t = 0$ of the laser pulse and the onset of morphology change is observed. It is referred to as t_1. Also, we have defined t_2 which is the elapsed time between the laser pulse and the completion of morphology change. SEM observations of our irradiated thin films have shown that changes in the optical reflectivity are mainly determined by the change of surface morphology and not by the changes of optical constants. Thus, the main information that the real time reflectivity measurements gives is the exact time for changes to start and finish and the net change in reflectivity. Table II shows these parameters for three specific samples: S2 (12 mW, 100 μs) which was the start of crystallization at the surface. It shows

TABLE II Measured reflectivity of Te–Se–Br thin films before and after irradiation; R: reflectivity before irradiation, ΔR: absolute reflectivity variation, ΔR/R: relative reflectivity variation, $t_1(t_2)$: elapsed time between time $t = 0$ of the laser and the on-set (completion) of morphology change

Sample	Structure	R (%)	ΔR (%)	ΔR/R (%)	t_1 (μs)	t_2 (μs)
S2 (12 mW, 100 μs)	Amorphous	37	− 0.4	− 1	–	–
S3 (62 mW, 5 μs)	Amorphous	35	− 3.5	− 10	4	9
S4 (25 mW, 100 μs)	Partly crystalline	36	− 11	− 31	7	108

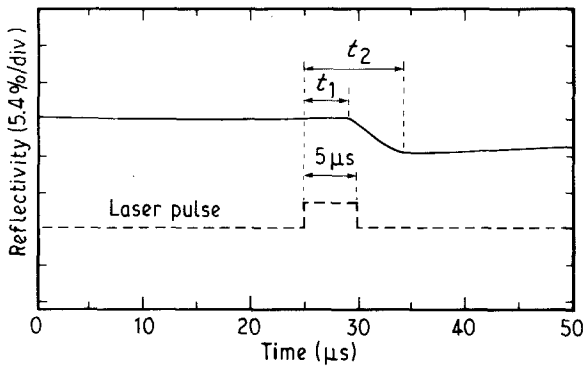

Figure 5 Reflectivity as a function of time for a Te–Se–Br thin film after a S3 (62 mW, 5 μs) laser pulse.

very little change (1%) as expected from the small surface rearrangement. The other two samples were chosen as examples of short and long irradiation times: In S3 (62 mW, 5 μs) and S4 (25 mW, 100 μs), one can notice that $(t_2 - t_1)$ is of the order of the laser pulse length (which can be understood by the calculations discussed below). This suggests that, for Regions II and III, the film morphology is changing continuously over a period equal to the pulse duration. Thus, in both μs regimes non-ablative physical and/or chemical processes induced by laser irradiation are relatively slow. In other words, fast reflectivity changes (< 100 ns for instance) are not to be expected when irradiating this Te–Se–Br system. This is also very well illustrated in Fig. 3 where the shape of Region II determined by the relation between the pulse length and power parameters, suggests that a significant increase of laser power will not dramatically decrease the pulse length needed for morphology changes.

It is interesting to compare these (25 mW, 100 μs) results with those at higher powers where ablation occurs. For 25 mW, the transformation is completed at 108 μs as reported in Table II. For the same 100 μs pulse width, powers of 35 and 45 mW induce ablation as expected from Fig. 3, which is complete after 79 μs and 37 μs, respectively.

In order to investigate the physical processes involved when the thin film is irradiated, we have carried out heat-flow calculations. The temperature of the centre of the irradiated area has been computed as a function of time by employing a program written by R. Kant [7]. We have considered a three layer system: Vacuum, the Te–Se–Br thin film and carbon-coated mica. Values of the thermal properties, specific heat and thermal conductivity can be found in the literature for carbon and mica [8]. For $Te_{30}Se_{50}Br_{20}$, we have measured the specific heat C_p from room temperature to 120 °C by means of DSC techniques. Absolute C_p values have been determined by using sapphire as a reference. For $T < 75$ °C (below T_g) the specific heat is constant and equal to 0.197; $K^{-1} g^{-1}$. For $T > 85$ °C, C_p is also constant but equal to 0.402; $K^{-1} g^{-1}$ in that case. This latter value has been used in the calculation. The Te–Se–Br thermal conductivity has been estimated from the literature to be 0.01 $W cm^{-1} K^{-1}$. Since direct crystallization of our $Te_{36}Se_{51}Br_{13}$, thin film has never been observed, the heat of crystallization was not included in the calculation. We have made the calculation for a constant 100 μs pulse length and 10 μm beam diameter with the absorbed laser power equal to 6, 12, 25, and 37 mW. These four sets of experimental conditions correspond, respectively, to the four points S1, S2, S4 and S6 in Fig. 3 which are representative of the four major regions: (I) No effect, (II) mostly amorphous, (III) crystalline, and (IV) ablated. The results are shown in Fig. 6. The maximum temperature in the centre of the irradiated area is equal to 200, 400, 820 and 1220 °C with respect to increasing power. These maxima are attained at the end of the pulse. The relationship between the chemical composition of our films after irradiation (Table I) and the heat flow calculations of Fig. 6 will be discussed in the next section.

4. Discussion

From Table I, one can notice that three major phenomena may occur during irradiation: An almost total

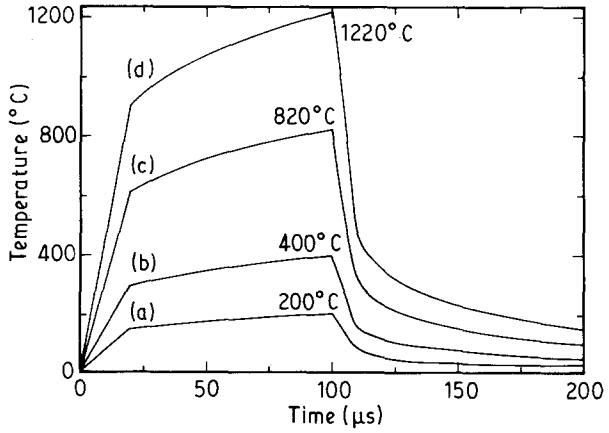

Figure 6 Calculated temperature versus time on the thin film surface, in the centre of the irradiated area. Pulse length: 100 μs. Absorbed laser power; (a) 6 mW, S1 (b) 12 mW, S2 (c) 25 mW, S4 (d) 37 mW, S6.

loss of bromine, partial loss of selenium, and crystallization of Te–Se solid solutions. The heat-flow calculations reported in Fig. 6 account well for the first two processes. Curve (a) in Fig. 6 is for a S1 (6 mW, 100 μs) irradiation which is observed to have no effect on the film morphology (see diagram in Fig. 3). The maximum temperature at the centre of the irradiated zone is calculated to be 200 °C. Melting of the film is not expected at that temperature. Crystallization may occur as shown in Fig. 2b, but the laser pulse is probably too short to allow a full glass-crystal transformation of our Te–Se–Br material to occur. However, a slight amount of bromine is probably already lost in this case. Curve (b) in Fig. 6 is for a S2 (12 mW, 100 μs) irradiation which induces large morphology changes but only scarce crystallization. The maximum temperature is calculated (Fig. 6) to be 400 °C. Since we know that this composition is completely melted at 300 °C in normal conditions, we may assume that the film is at least partially melted. In Table III, we have listed the melting and boiling points of Te, Se, Br_2, Te–Br and Se–Br stable compounds in normal conditions (This Table should be used as a guideline only). Thus, at 400 °C Br_2 and selenium bromide compounds, if any, would certainly evaporate from the melt. It is also possible that evaporation of some Se (and perhaps some $TeBr_4$) occur. However, we can conclude that the first morphology changes are due to the evaporation of some bromine and to some partial melting process, resulting in surface damage. Curve (c) in Fig. 6 is for a S4 (25 mW, 100 μs) irradiation which induces crystallization. The maximum temperature is found to be 820 °C which is above all the transition temperatures in Table III (except Te). Considering that at this temperature the film is totally melted, one can predict an important loss of Br and Se for the irradiation condition S4. This is effectively demonstrated by chemical analysis, as reported in Table I. S4 has also probably lost a small amount of Te. Also from Table I, it is to be noted that the Se content increases from the centre to the edge of the spot. This is due to the Gaussian laser beam which induces a temperature gradient with a consequent diffusion Se concentration gradient. For bromine on the other hand, even on the edge of the irradiated spot the temperature is higher than the Br_2 boiling point. The heat flow calculations can also be used to describe the real time reflectivity data (Table II). The delay, t_1, is expected to be due to the delayed rise in the film temperature. For S4, the observed delay of $t_1 = 7$ μs would be the time for the centre of the film to reach $\simeq 250$ °C. Note that the surface stays at a high temperature (Fig. 6) for a time interval approximately equal to the laser pulse length, in accordance with the empirical observation noted above. Curve (d) of Fig. 6 is for a S6 (37 mW, 100 μs) pulse which causes thin film ablation. The maximum calculated temperature (1220 °C) is higher than the boiling points listed in Table III, including that of amorphous tellurium. In fact, evaporation is not a necessary condition since ablation of tellurium compounds has been explained by melting and successive hole formation driven by surface tension gradients [9]. Thus, the heat flow calculations well account for the general features of the behaviour observed in our experiments. Although the above description accounts for the observed behaviour, we can expect quantitative variations because of differences between the thermal analysis which is done under thermodynamically stable conditions in a bulk sample and the short pulse laser irradiation of thin films which takes place in metastable conditions.

We have been able to determine the first step in the crystallization process: The random dendritic structures observed in Fig. 4a which can be described by computer simulation of fractal network formation. [10]. The model assumes a diffusion-limited aggregation of single particles and/or clusters in a two dimensional base-lattice. This is consistent with the surface growth that is observed. From a more physical point of view, we believe that the filamentary growth observed is due to complex vapour–liquid–solid (VLS) mechanism based on the process proposed by Wagner and Ellis [11] for the growth of silicon whiskers. Our material has three components with such different transition temperatures that the VLS state is induced when the laser beam irradiates the sample.

In Fig. 7, we have portrayed the Te–Se–Br ternary diagram. (A) is a glass-forming region where DSC curves do not exhibit any crystallization peaks. (B) is

TABLE III Melting and boiling temperatures of tellurium, selenium, bromine and their compounds in normal conditions; T_m: melting temperature, T_b: boiling temperature, (d): compound decomposes

Compound	T_m (°C)	T_b (°C)
Br_2	− 7.2	58.8
Se	217	684.9
Se_2Br_2	–	227(d)
$SeBr_4$	75(d)	–
Te (amorphous)	449.5	989.8
Te (crystalline)	452	1390
Te_2Br	225(d)	–
$TeBr_4$	380	421(d)

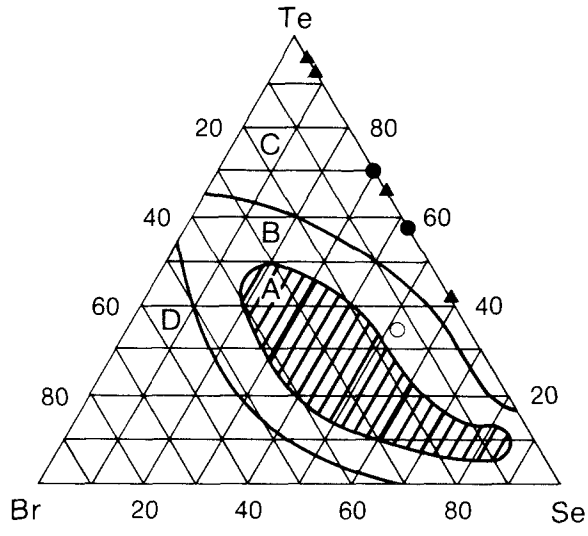

Figure 7 Te–Se–Br ternary system; (○) as-deposited glass, (▲) crystalline after irradiation, (●) amorphous after irradiation. Regions A, B, C and D are explained in the text.

also a glass-forming region but crystallization peaks are present in the DSC curves. In regions (C) and (D), only crystals are formed. One should be aware that this diagram has been obtained in stable conditions by refining the melted materials at 300 °C for several hours and then, slowly cooling them down to room temperature [1]. We have also shown in the diagram the compositions listed in Table I which result from the laser irradiations. Even though these compositions are all located in region (C) where only crystals are expected, both (●) amorphous and (▲) crystalline phases are found. Furthermore, which one is formed appears uncorrelated to the composition, but strongly correlated to the laser pulse length: amorphous phases are obtained with pulses equal to 5 μs, while crystals are formed with 100 μs and 100 ms irradiations. From the heat-flow calculations we deduce that after a (62 mW, 5 μs) pulse, the cooling rate is equal to 320 °C μs^{-1}. while for a (25 mW, 100 μs) pulse it is equal to 34 °C μs^{-1}. In other words, every composition located in region (C) including the Te–Se binary is very likely, provided that the power absorbed by the system is sufficient, to crystallize for pulses greater or equal to 100 μs, and to remain amorphous for shorter pulses.

5. Conclusions

Pulsed laser irradiation of $Te_{36}Se_{51}Br_{13}$, films has been shown to induce almost complete evaporation of bromine and melting of the remaining alloy whose concentration of Se is variable depending on irradiation conditions. The general results are consistent with heat-flow calculations over the range of parameters studied. The Te–Se alloys formed after irradiation are amorphous or crystalline depending not on their composition, but on the quenching rate which is controlled by the parameters of laser pulse length and power. Furthermore, we have been able to establish that the crystallization starts with surface filamentary growth exhibiting fractal network formation. With higher laser energy it tends to coalesce to form three dimensional metallic crystals.

Acknowledgements

The authors thank C. Echer of the National Center for Electron Microscopy, Lawrence Berkeley Laboratory for his help with EDS. The assistance of K. Roche and R. Savoy of IBM for reflectivity measurements and microprobe analysis, respectively, is greatly appreciated.

References

1. X. H. ZHANG, G. FONTENEAU and J. LUCAS, *J. Non-Cryst. Solids* **104** (1988) 38.
2. J. LUCAS, *Mater. Res. Soc. Symp. Proc.* **152** (1989) 41.
3. X. H. ZHANG, G. FONTENEAU, J. LUCAS, A. PERRIN, Z. Z. LI and M. SERGENT, *Mater. Sci. Forum* **32–33** (1988) 453.
4. R. KNIEP, D. MOOTZ and A. RABENEAU, *Angew. Chem. Int. Ed.* **12** (1973) 499.
5. E. GRISON, *J. Chem. Phys.* **19** (1951) 1109.
6. D. M. CHIZHIKOV and V. P. SHCHASTLIVYI, in "Selenium and Selenides" (Collet's, London, 1968) p. 361.
7. R. KANT, *J. Appl. Mechan.* **110** (1988) 93.
8. Y. S. TOULOUKIAN, R. W. POWELL, C. Y. HO and P. G. KLEMENS, in "Thermophysical Properties of Matter" (IFI/Plenum, New York, 1970) p. 274.
9. K. RUBIN, Private communication.
10. P. MEAKIN, *Phys. Rev. Lett.* **51** (1983) 1119.
11. R. S. WAGNER and W. C. ELLIS, *Appl. Phys. Lett.* **4** (1964) 89.

Received 18 January
and accepted 16 May 1990